Glycine in an Electronically Excited State: Ab Initio Electronic Structure and Dynamical Calculations

Eva Muchová,[†] Petr Slavíček,[‡] Andrzej L. Sobolewski,[§] and Pavel Hobza*[,†]

Institute of Organic Chemistry and Biochemistry, Academy of Sciences of the Czech Republic and Center for Biomolecules and Complex Molecular Systems, Flemingovo nám. 2, 166 10 Prague 6, Department of Physical Chemistry, Institute of Chemical Technology, Technická 5, 166 28 Prague 6, and Institute of Physics, Polish Academy of Sciences, PL-02668, Warsaw

Received: February 22, 2007; In Final Form: April 3, 2007

The goal of this study is to explore the photochemical processes following optical excitation of the glycine molecule into its two low-lying excited states. We employed electronic structure methods at various levels to map the PES of the ground state and the two low-lying excited states of glycine. It follows from our calculations that the photochemistry of glycine can be regarded as a combination of photochemical behavior of amines and carboxylic acid. The first channel (connected to the presence of amino group) results in ultrafast decay, while the channels characteristic for the carboxylic group occur on a longer time scale. Dynamical calculations provided the branching ratio for these channels. We also addressed the question whether conformationally dependent photochemistry can be observed for glycine. While electronic structure calculations favor this possibility, the ab initio multiple spawning (AIMS) calculations showed only minor relevance of the reaction path resulting in conformationally dependent dynamics.

1. Introduction

In recent years, a great deal of attention has been paid to the photochemistry of nucleic acids and their molecular components. Concerted experimental and theoretical effort has been made to reveal the mechanism of DNA photostability and radiation protection.[1,2] State-of-the-art spectroscopy experiments in the gas phase using fluorescence, resonance-enhanced multiphoton ionization (REMPI) detection, as well as IR/UV double-resonance spectroscopy have provided new insight into the photochemistry and photodynamics of the nucleobases.[3−7] The experiments have been accompanied by theoretical investigations utilizing the whole toolbox of computational chemistry ranging from quantum chemistry to quantum dynamics.[8−12]

The photochemistry of proteins, peptides, and amino acids, however, has not been as extensively mapped out. The reason is that amino acids are generally poor chromophores, which makes the experiments more demanding. The photochemistry of amino acids and proteins also does not interfere with their biological function as much as in the case of nucleic acids.

Peptides, on the other hand, can also undergo interesting photoactivated processes. In the case of glycine trimer and pentamer, for instance, the suggested excited-state deactivation mechanism is strikingly similar to that found in nucleic acids.[13] It is, of course, still possible that the proposed mechanism represents only a minor reaction channel. Unfortunately, even glycine trimer is conformationally too complex to be able to understand all its photochemical details.

In order to gain insight into the photochemistry of peptides, we first attempted a theoretical exploration of the simplest peptide unit—glycine.

A known photochemical behavior of amines and carboxylic acids may provide us with a hint to the possible pathways. The first ultraviolet absorption band of amines involves excitation of a nitrogen lone pair electron to a 3s Rydberg orbital. In the excited state the molecule can decompose via various channels, among which N−H bond dissociation is dominant, accounting for more than 75% of the yield.[14−16] The theoretical work showed that the excited-state potential-energy surface (PES) with respect to the N−H coordinate is characterized by a small barrier at a shorter distance and a conical intersection with the ground state at a larger distance.[17,18] The excited-state products lie above the excitation energy; thus, the dissociating molecules are funneled through the conical intersection to the ground state.

In the case of acetic acid, its photochemistry is complicated and not all channels are fully understood at present. The photochemical reactions have been the subject of numerous experimental investigations[19−22] and theoretical studies.[23−26] Those experiments revealed that the dominant pathway for CH_3-COOH is the C−OH bond dissociation yielding CH_3CO and OH (in the range of 200−220 nm). According to the theoretical calculations the first excited state is of $n_O \rightarrow \pi^*_{CO}$ character. From this state there are three possible radiationless routes: internal conversion (IC) to the ground state, intersystem crossing (ISC) to the lowest triplet state (T_1), and direct dissociation on the S_1 surface.[23] The S_1/S_0 crossing point was ascertained to be higher in energy than both the S_1/T_1 point and the saddle point for cleavage of the C−O bond. The S_1/S_0 crossing point is also nearly inaccessible in terms of energy (even with excitation at 200 nm). The S_1/T_1 point has a geometry similar to that of the S_1 minimum, and the barrier for the transition from S_1 to T_1 is approximately 0.3 eV (approximately 0.4 eV lower than the barrier for direct dissociation on S_1).[23] Even though ISC is a spin-forbidden process, the present calculations suggest that ISC competes with the S_1 direct dissociation reaction.[23]

Amino acids contain both amino and carboxyl groups. The dynamics can thus be dominated by either ultrafast processes

* To whom correspondence should be addressed. E-mail: pavel.hobza@uochb.cas.cz.

† Academy of Sciences of the Czech Republic and Center for Biomolecules and Complex Molecular Systems.

‡ Institute of Chemical Technology.

§ Institute of Physics.

10.1021/jp071483x CCC: $37.00
Published on Web 05/27/2007

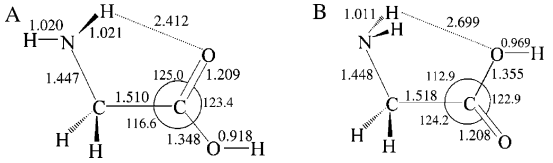

Figure 1. Geometries of the ground-state minima for conformers A and B computed at the MP2/cc-pVTZ level.

resulting from the properties of the amino group on the one hand or slow processes due to the carboxyl moiety on the other.

Even such a simple molecule as glycine has a rather rich conformational space in the ground state. As will be discussed in section 3, glycine is a floppy molecule with different hydrogen-bonded patterns for different minima (see Figure 1 and Figure 1S). Although the interconversion barriers for glycine are low (about 1 kcal/mol, 0.04 eV),[27] it is possible to detect various conformers experimentally.[28,29] At the same time, some of the photochemical processes in glycine are expected to occur on a femtosecond time scale. The photochemical dynamics in this case are then highly nonstatistical. Therefore, we addressed the question of whether conformationally specific dynamics can be observed after photoexcitation. For some conformers one of the amino-group hydrogens is located between the nitrogen and the carbonyl oxygen. This would suggest a possibility of intramolecular excited-state hydrogen transfer, which is closely analogous to the hydrogen transfer described for a glycine trimer. For other conformers the same process would require a considerable conformational change in the excited state that would presumably occur on a larger timescale. This type of behavior has been previously reported by Gerber et al. in the case of photoionization of glycine.[30]

Electronic structure theory methods have been widely used over the last years to reveal photochemical reaction mechanisms.[31−36] Recently, these studies have been moving from single molecules to reactions in a condensed phase[37,38] or in a protein environment.[39−41]

Quantum chemistry is a basic tool for understanding photochemical mechanisms. With the use of electronic structure methods it is possible to locate minima, transition-state structures, and (conical) intersection seams, which play a major role in photochemical mechanisms.[42−44] A whole range of theoretical methods describing excited states exists.[45] Some of these methods, e.g., time-dependent DFT of CC2, are highly accurate for a comparatively low computational price. However, the scope of these methods is often limited.[46,47] To describe consistently the whole relevant potential-energy surface (PES), including regions of conical intersections, multireference-based methods have to be employed. Among these the complete active space (CAS) SCF method represents the essential minimum for at least a qualitative description of the PES. To verify the CASSCF calculations, it is necessary to include dynamical correlation. This can be done at the multireference configuration interaction (MRCI) level or in a less demanding way via second-order perturbation theory (CASPT2).[48,49]

Quantum-chemical calculations have two major drawbacks. First, they only provide local information about the PES, which is a complicated multidimensional function of nuclear coordinates. As we are limited to low-dimensional cuts of the PES, the proposed mechanism may be governed by our prejudice. Second, no direct information on the duration of the photochemical process is acquired from quantum-chemical calculations. By solving equations for the motion of atomic nuclei, i.e., by performing molecular-dynamics simulation, it is possible to circumvent these two limitations. The PES describing the interaction between nuclei is preferably calculated at the ab initio level on the fly. Since fully quantum treatment of the nuclear dynamics within the ab initio context is obviously impractical, semiclassical approaches have to be utilized. Among these, the surface hopping algorithm[50−52] and Ehrenfest dynamics[53,54] are the most frequently used. Implementation of Tully's algorithm in the framework of Car−Parrinello molecular dynamics has been reported.[55,56] Even though these methods are suitable for the description of many systems, they sometimes provide poor results due to an insecure theoretical basis and slow convergence.[57] In this study, we employed the full multiple spawning (FMS) method of Martínez and Ben-Nun.[58−60] Some details of this approach are briefly discussed in section 2.

The paper is organized as follows: In Computational Methods section the employed computational tools are discussed. It is followed by the Results section in which the detailed results are provided. In the Discussion section the possible reaction pathways are revealed. The investigation of the possible reaction channels from the ab initio molecular-dynamics point of view is also provided in this section. Finally, the main points of the study are summarized in the Conclusions section.

2. Computational Methods

Electronic Structure Methods. The electronic structure methods for the rigorous description of the PES need to be flexible enough to accommodate the multiconfigurational character of the wave function in regions far from the Franck−Condon (FC) points. It is crucial especially when the breaking of bonds or bond rearrangement occurs. This is supposed to be the case with glycine photodynamics.

The CASSCF method is the cheapest method that fulfills these requirements. In our study, the CASSCF method was chosen as an efficient tool for mapping the topography of the PES. Over the years, the geometries obtained by CASSCF have been proven to be accurate. This method is also the method of choice for dynamical calculations. A reliable CASSCF active space has to be designed in such a way that (i) it provides accurate results in the FC region, (ii) it is consistent with the benchmark values obtained by MRCI and CASPT2 for barrier heights and energies of the crossing points, and (iii) it is stable and efficient in dynamical calculations. The best active space does not have to be necessarily the most chemically intuitive or largest possible. It is, however, necessary to mention that the correct picture is the one obtained by employing both large active space *and* correlation effects.

The survey on energies of the FC point and various important points on the PES obtained using different active spaces and methods is provided in Tables 1 and 2. According to these data, the active space that has best met all the requirements is the CAS(6/7) using the basis defined below. This active space containing in the FC point π_{CO}, the lone pair on nitrogen and carbonyl oxygen π_{CO}* and three Rydberg orbitals provides correct qualitative results in all relevant parts of the PES. For most of the results there is also a reasonable quantitative agreement with the more accurate CASPT2 and MRCI results. In the terminology we used in this paper SA-3-CAS(6/7) denotes full CI in the active space containing six electrons in seven orbitals. The orbitals are optimized to minimize the state-averaged energy of the lowest three singlet states.

In order to refine the energetics, we traced the PES along the paths predicted by CASSCF employing the CASPT2 and MRCI methods. In this way we were also able to control the consistency between the accurate results from MRCI and CASPT2 as well as the dynamical results obtained at a lower level of theory.

TABLE 1: Vertical Excitation Energies (in eV) for Conformers A and B Using Various Levels of Theory[a]

	A		B	
	$n_O \rightarrow \pi^*_{CO}$	$n_N \rightarrow 3s$	$n_O \rightarrow \pi^*_{CO}$	$n_N \rightarrow 3s$
CASSCF(6/6)	6.21	6.58	6.43	6.59
CASSCF(6/7)	6.22	6.35	6.22	6.60
CASSCF(8/8)	6.21	7.01	6.05	6.52
CASSCF(10/10)	5.99	6.52	6.02	6.31
CASPT2(6/6)	5.73	6.05	5.79	6.00
CASPT2(6/7)	5.73	5.99	5.79	5.99
CASPT2(8/8)	5.71	6.15	5.70	6.02
CASPT2(10/10)	5.85	6.05	5.72	6.14
MRCI(6/6)	6.04	6.27	6.06	6.33
CASPT2/ANO-L+R[b]				
CCSD/aD(T)[c]			5.88	6.09

[a] The basis set employed in all the calculations was 6-31G* augmented by diffuse and polarization functions on the hydrogen atoms of the amino group. The experimental excitation energy refers to the vacuum UV spectra of a series of poly(α-amino acid)s, ref 70. [b] Reference 72. [c] Reference 71.

In this particular case, selection of the basis set represents a difficult task. On one hand, the basis set should contain polarization and diffuse functions for N−H bond dissociation (the hydrogen-transfer channel leads to the identical requirement on the basis set) to be described correctly and, on the other, suitable for efficient and stable dynamical calculations. The next requirement is also a reliable physical justification. As larger basis sets combined with a relatively small active space can lead to spurious effects due to unbalanced description. We used the 6-31G* basis set augmented by diffuse and polarization functions on the hydrogen atoms of the amino group. The results obtained with this basis set are quantitatively the same as those obtained by employing 6-31G** augmented by diffuse and polarization functions on a nitrogen atom or aug-cc-pVDZ with added s and p diffuse functions with a coefficient of 0.02 on a nitrogen atom (as used in the work of Domcke and Sobolewski[61]). The latter-mentioned basis sets, however, led to instabilities when the PES was scanned. The results obtained by employing our basis set are also in agreement with the results obtained using differently constructed basis set by other authors.[71,72]

So as to trace the PES, we located minimum-energy structures and minimum-energy conical intersections (MECIs), which was in both cases done using the CAS(6/7) wave function with the algorithm as implemented in MolPro, a package of ab initio programs.[62] In order to gain more insight into the character of the PES between the FC region and MECIs we performed linear interpolation of coordinates (LICC), which was done in Cartesian space after the two structures had been suitably oriented. The interpolation in internal coordinates was done with the aim of checking whether the shape of the curves was not an artifact of interpolation in Cartesian space. We also performed a relaxed PES scan. In this case, the driving coordinate remained fixed while all the remaining degrees of freedom were optimized.

All ground-state geometries were calculated at the MP2 level with the cc-pVTZ basis set, and this was the same level as that used for evaluation of ground-state harmonic vibrational frequencies in dynamical calculations.

All the presented electronic structure calculations were carried out using the MolPro.[62]

Dynamics. We used the full multiple spawning method to perform dynamical simulations. In this approach the nuclear wave function is treated explicitly and nonadiabatic effects leading to population transfer between electronic states are taken into account. The FMS method expresses the nuclear wave function in the I^{th} electronic state in a form of an adaptive basis set of moving Gaussian functions

$$\chi_I(R;t) = \sum_{j=1}^{N_I(t)} C_j^I(t) G_j^I(R; \bar{R}_j^I(t), \bar{P}_j^I(t), \gamma_j^I(t), \alpha_j^I)$$

These functions are parametrized by mean position ($\bar{R}$) and momentum ($\bar{P}$) vectors which evolve according to classical equations of motion. Gaussian functions are further specified by a width α (held constant in our calculations) and phase γ (calculated in a semiclassical way). The time evolution of complex expansion coefficients in the expansion into the Gaussian basis set is determined using the time-dependent Schrödinger nuclear equation. In this way, the method is exact in the limit of the infinite basis set. At the same time, only local information (i.e., energies and gradients) is needed for the calculation using a saddle-point approximation for evaluating matrix elements. This approximation is possible due to the localized nature of the Gaussian basis. This allows avoidance of the tedious preparation of analytically interpolated PESs. Gaussian localization also leads to practically linear scaling of the method, where the number of the basis set for the matrix element between distant Gaussian functions can be neglected.

To account for nonadiabatic transitions, we need to trigger a new trajectory on the PES of a different state whenever nonadiabatic matrix elements between the parent state and some other state exceed a certain value. This procedure is called "spawning". The basis set thus expands adaptively throughout the simulation. The newly created basis is coupled to all other basis functions. This enables population transfer. Details of the FMS method together with a discussion of various technical issues can be found in a number of review articles.[66−68]

Since we simulate a system at 0 K, it would be in principle possible to run merely a single FMS simulation with a wave function expanded over a large number of Gaussian functions which mutually interact. Instead, for practical reasons, we sampled the initial wave function using a Wigner distribution of a ground-state vibrational wave function. Various trajectories then evolve independently (but spawned trajectories are still coupled to the parent trajectories). A velocity Verlet algorithm with a time step of ∼0.25 fs was used as an integrator, with the total time of the simulation being 500 fs. The widths of the Gaussian functions were chosen to be 6 $bohr^{-2}$ for hydrogen atoms and 30 $bohr^{-2}$ for all heavy atoms (C, N, O). We sampled both the S_1 and the S_2 state because they are close in energy—10 initial Gaussians for each state and conformer. The initial harmonic wave function (i.e., vibrational frequencies) was calculated at the MP2 level of theory with the cc-pVTZ basis set. Initial positions and momenta were obtained by a Monte Carlo sampling of a corresponding Wigner distribution. In the calculations the CAS(6/7) wave function and basis set 6-31G* augmented by diffuse and polarization functions (6-31++G**) on the hydrogen atoms of the amino group was used.

The dynamical calculations were performed with the FMSMolpro code,[63] a synthesis of an FMS dynamical code and MolPro.[62]

3. Results

Conformational Space of Glycine. Great experimental[28,29] and theoretical[27,64] effort has been made to fully describe the conformational behavior of glycine. The flexibility of the molecule leads to a large number of rotational conformers that are very close in energy and separated by small interconversion barriers. The structures together with relevant geometrical parameters are depicted in Figure 1 (A and B) and Figure 1S

TABLE 2: Energies (in eV) of Important Points on the PES for Conformers A and B Calculated at Different Levels of Theory[a]

	A			
	adiab. exc. S_1	S_1/S_0 C═O stretch MECI	S_1/S_0 NHD MECI	S_1/S_0 HT MECI
CASSCF(6/6)	3.75	7.96	5.79, 5.88	4.83
CASSCF(6/7)	3.89	8.29	5.08, 5.24	4.54
CASSCF(8/8)	4.03	6.40	4.55, 4.91	4.64
CASSCF(10/10)	2.98	8.02	4.17, 4.25	5.18
CASPT2(6/6)	4.70	7.18	4.96, 5.10	4.99
CASPT2(6/7)	4.69	7.15	4.73, 4.76	4.89
CASPT2(8/8)	4.71	5.01	4.98, 5.13	5.06
CASPT2(10/10)	4.65	7.18	5.25, 5.30	4.83
MRCI(6/6)	4.61	7.36	5.40, 5.57	4.80
	B			
	adiab. exc. S_1	C═O stretch MECI	NHD MECI	
CASSCF(6/7)	3.29	7.10	5.13, 5.53	
CASPT2(6/7)	4.61	6.81	5.02, 5.06	
MRCI(6/6)	4.57	6.87	5.14, 5.48	

[a] All calculations were carried out on the geometries obtained by SA-3-CAS(6/7)SCF optimization or the conical intersection search using the same wave function. In all cases, the combined basis set (6-31G* augmented by diffuse and polarization functions on the hydrogen atoms of the amino group) was employed.

(C and D). Structure C represents the global minimum, and structures A, B, and D are the lowest energy conformers. The interconversion barriers to the global minimum are within the range 0.01−0.12 eV (0.23−2.69 kcal/mol) at the MP2/aug-cc-pVDZ level and published in ref 27.

There are three types of hydrogen bonds in the glycine molecule: N−H···O═C (conformers A and conformer C), N−H···O(H)−C (conformer B), and N···H−O (conformer D). For further mechanistic study we considered two conformers—A and B—the details are explained bellow.

Vertical Excitation Energies. Experiments on glycine in the gas phase have not been reported yet to the best of our knowledge. In the literature, the spectra of aliphatic amino acids in solution[65,66] and thin layers of amino acids and their di- and tripeptides[67] have been presented. The CD spectrum of several amino acids was measured by Snyder et al.[68] McMillin at al.[69] reported the vacuum ultraviolet spectra of a series of poly(α-amino acid)s; far ultraviolet (down to 115 nm) absorption spectra were recorded by Inagaki.[70] Electronic spectra of gas-phase glycine have been analyzed theoretically by Osted el al.[71] and Serrano-Andrés et al.[72] In these theoretical papers only one conformer was taken into account. These results are provided for the sake of comparison in Table 1.

The vertical excitation energies for conformers A and B are collected in Table 1. The results for conformers C and D are provided in Table 1S. The lowest state is known to be the $n_O \rightarrow \pi^*_{CO}$ transition from the lone pair localized on the carbonyl oxygen atom to the π^*_{CO} antibonding orbital. The excitation energy is almost the same as in the case of carboxylic acids (5.88 eV according to Osted et al.[71] and 6.06 eV according to our calculations for glycine; 5.98 eV for acetic acid according to Osted et al.[71]). The second lowest state is calculated to be of $n_N \rightarrow$ 3s character. The experimental value in Table 1 refers to the vacuum ultraviolet spectra of a series of poly(α-amino acid)s.[70] As the two lowest-lying states are close in energy (see Table 1), the transitions are found to be of a partially mixed character.

From Tables 1 and 1S it is clear that the vertical excitation energies are dependent on the conformation. The results obtained with the aid of the methods, which include dynamic correlation, are different from the CASSCF results with various active spaces. In general, the CASSCF values are higher than the MRCI values (with the exception of the 10/10 active space, which yields results closer to the MRCI method); the CASPT2 method, on the other hand, underestimated the values when compared with the MRCI method. For conformer D the difference between the CASSCF and the more accurate CASPT2 and MRCI energies is the greatest (see Table 1S).

Values of oscillator strengths found in the literature vary, ranging from 0.001 and 0.005 for the two lowest-lying states in the work by Serrano-Andrés et al.[72] to 0.00053 and 0.01247 in the work by Osted et al.[71] On the basis of our calculations the transition dipole moments of the two lowest-lying states should be similar as a result of the partial mixing of the states mentioned above. Partial mixing of transitions was also noticed by Osted et al.[71] In order to provide a correct picture of the processes taking place after excitation, we investigated both states, and these states were also populated in dynamical calculations.

The adiabatic excitation energies of the lowest excited singlet states are shown in Table 2 (for conformers A and B). The MRCI and CASPT2 results are comparable and agree well with the values obtained for acetic acid.[23] The CASSCF method, on the contrary, yields results systematically underestimated by about 1 eV.

Excited-State Potential-Energy Surfaces of Glycine. While examining the processes following photoexcitation of glycine we restricted our attention to two of the conformers—A and B. For conformers A and C the possibility of hydrogen transfer was anticipated. The N−H···O distance is, however, shorter in the case of conformer A than in conformer C, which makes the conditions for hydrogen transfer in conformer A even more favorable than in C. Note, however, that important parts of the excited-state PES were identical for both conformers. As a result, the dynamical behavior is similar too.

For conformers B and D, on the other hand, hydrogen transfer would have had to be preceded by a considerable conformational change. Therefore, for further study, we selected conformer B as a structure whose hydrogen-bond pattern of N−H···O(H)C type is not suitable for hydrogen transfer. Both conformers B and D would serve for comparing the photochemical behavior in the same manner; however, conformer B showed a better numerical stability when calculating the whole potential-energy surface and subsequent dynamics.

The geometries of the most important points on the PES obtained at the CAS(6/7) level are summarized in Figure 2. The

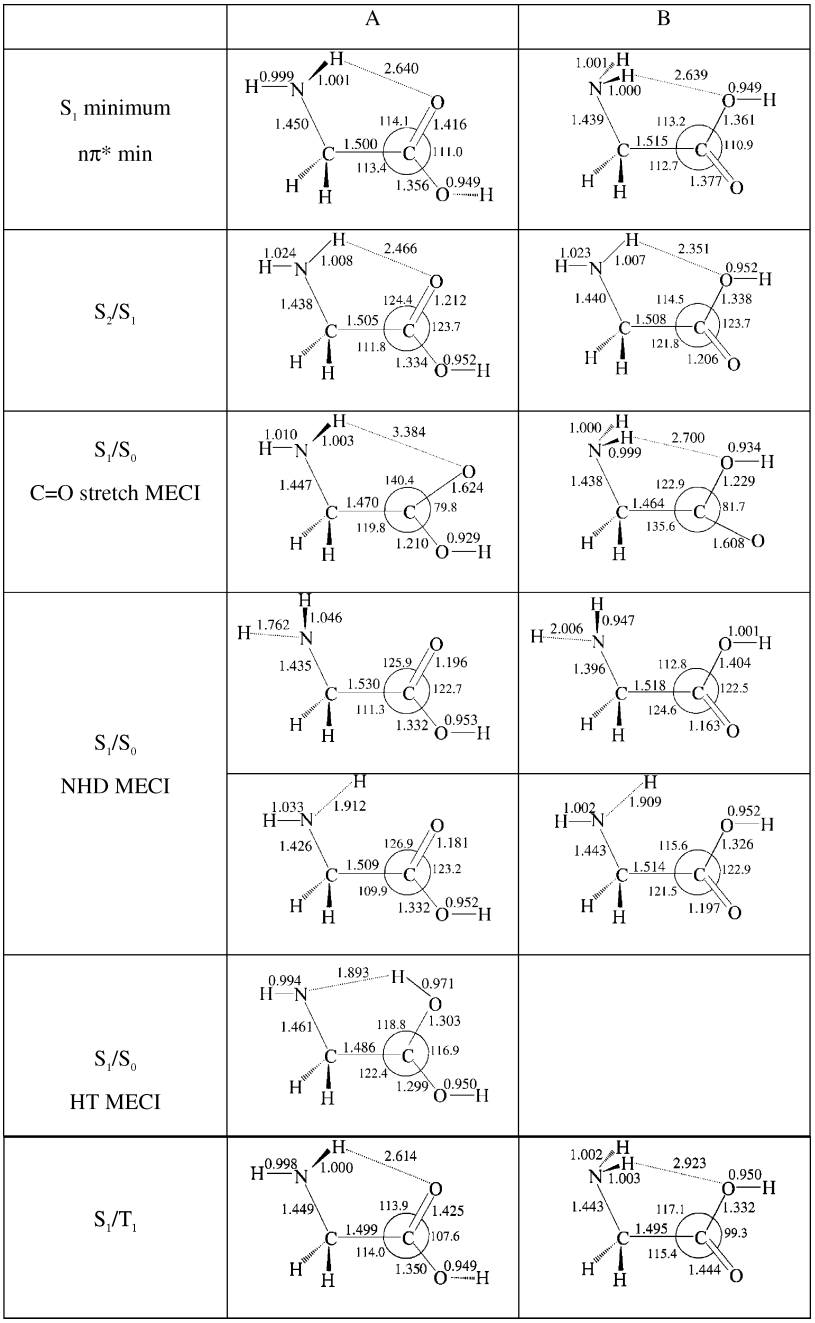

Figure 2. Geometries of important points on the PES for conformers A and B. The structures were optimized at the CAS(6/7) level using the basis set 6-31G* augmented by diffuse and polarization functions on the hydrogen atoms of the amino group.

energies of these points on the PES calculated for both conformers at various levels of theory are presented in Table 2. The energy differences between these points on the PES of conformers A and B obtained at the MRCI(6/6), CASPT2(6/7), and CAS(6/7) levels of theory are schematically depicted in Figure 3.

As previously mentioned, the first transition is dominantly of $n_O \rightarrow \pi^*_{CO}$ character in the FC region. Promotion of one electron to the π^*_{CO} antibonding orbital gives rise to pyramidalization of the carboxyl heavy-atom backbone and C═O bond elongation (1.22 Å in the ground state to ∼1.40 Å in the nπ*-state minimum). The nπ*-state minima for conformers A and B are presented in Figure 2. The geometries of the carboxyl moiety presented in Figure 2 are similar to the nπ*-state minimum found for acetic acid.[23] Extensive geometrical changes are reflected in the difference between vertical and adiabatic excitation energies (1.43 and 1.49 eV at the MRCI level for conformers A and B, respectively). The global minimum on the nπ* state, unlike in the ground state, is of a B-structure type (labeled as B S_1 minimum in Figure 2). At the MRCI(6/6) level the global minimum is more stable than the nπ*-state minimum for conformer A—by about 0.04 eV (1 kcal/mol). The interconversion barrier between the nπ*-state minima of conformers A and B is less than 0.16 eV (4 kcal/mol) at the MRCI-(6/6) level.

The nπ* diabatic state is connected to the S_0 state via a conical intersection seam with a stretched C═O bond. The S_1/S_0 MECIs for the C═O stretch (C═O MECIs) between the ground state and nπ* state are presented in Figure 2 for conformers A and B (the structures marked as C═O stretch MECI). The C═O bond is elongated to ∼1.65 Å. The heavy-atom backbone of the carboxyl group is extensively distorted when compared to S_1/S_0 MECI in acetic acid. At the MRCI-(6/6) level the C═O stretch MECIs are 2.75 and 2.30 eV higher

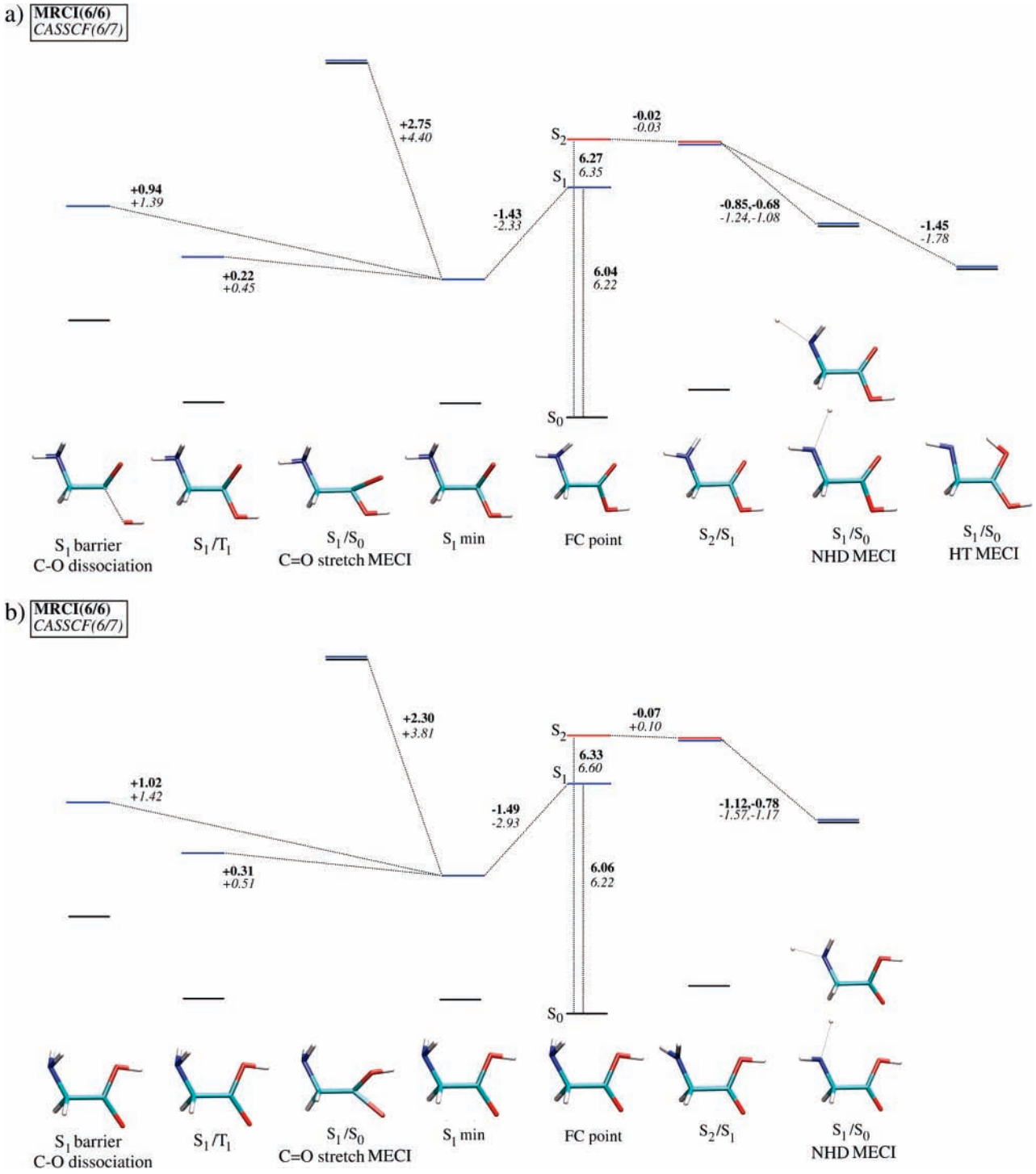

Figure 3. Diagram of energy differences for important points on the PES obtained at the MRCI(6/6) and SA-3-CASSCF(6/7) levels for conformers A (a) and B (b). Zero is defined as the energy of the ground-state minimum of appropriate conformer. The black line denotes the ground state S_0, the blue line is S_1, and the red line is S_2.

in energy (for conformers A and B, respectively) than the nπ*-state minima and 1.32 and 0.81 eV (for conformers A and B, respectively) higher than vertical excitation energies to S_2 (see Figure 3). At the CAS(6/7) level the energy difference between the nπ*-state minima (for conformers A and B) and the C═O stretch MECIs (for conformers A and B) are even bigger, which is a result of the overstabilization of the nπ*-state minima at the CASSCF level.

As in the case of acetic acid, the nπ*-state minima (of conformers A and B) have a very similar geometry to the S_1/T_1 crossing points (for conformers A and B, see Figure 2). The energies of the S_1/T_1 crossing points are only 0.31 and 0.22 eV higher for conformers A and B, respectively, than the nπ*-state minima (of conformers A and B). This might suggest that the ISC from the S_1 to T_1 states can occur to a noticeable extent.

The nπ* state correlates adiabatically with the ground-state fragments NH_2CH_2CO and OH in a manner similar to acetic acid. The transition state for the C−O(H) bond cleavage has the C−O(H) bond length of 1.753 Å (structure not presented), so the bond is nearly broken. The energy of the transition state is 0.94 eV above the nπ*-state minimum for conformer A at the MRCI(6/6) level.

The character of the S_2 state in the FC region is $n_N \rightarrow 3s$. As the N−H bond stretches, the original Rydberg 3s orbital mixes

with the N−H σ^* orbital and the character of the state changes to $n_N \rightarrow \sigma^*$. For both conformers the S_2 state is in the FC region in proximity to S_2/S_1 MECI, which is also a minimum on the S_2 PES. The geometries of the S_2/S_1 MECIs are depicted in Figure 2 (for conformers A and B). The amino group is planar, which is in agreement with the photochemical behavior of alkyl amines. The relative energies of the S_2/S_1 MECIs (for conformers A and B) are collected in Figure 3. The S_2/S_1 MECIs are at the MRCI(6/6) level only 0.02 and 0.07 eV (for conformers A and B, respectively) lower in energy that the S_2 vertical excitation energies (for conformers A and B).

A wave packet prepared in the S_2 state by optical excitation splits at the S_2/S_1 MECI between the nπ^* and nσ^* states. It is known that the nσ^* state is dissociative with respect to the N−H bond. The N−H bond lengthening can result in two processes: (i) N−H bond dissociation and (ii) hydrogen transfer to the carboxyl group (if the hydrogen-bond pattern is suitable, as is the case of conformer A). Both routes are barrierless when starting from S_2.

In the case of N−H bond dissociation, the nσ^* state correlates with the ground-state products ^{2}S H and NH−CH_2COOH. The structures of the S_1/S_0 MECIs for N−H bond dissociation (NHD MECI) are depicted in Figure 2 (for conformers A and B), and the energies are summarized in Table 2. The relative energies of the NHD MECIs (for conformers A and B) are presented in Figure 3. For each of the conformers A and B one structure was located in which the dissociating hydrogen was oriented toward the carboxyl group and one in which the outgoing hydrogen atom pointed to the opposite side (see Figure 2). The latter one was energetically more stable by 0.17 eV for conformer A and 0.34 eV for conformer B (at the MRCI(6/6) level). The structures of NHD MECIs are characterized by N−H bond lengths ranging from 1.8 to 2.0 Å. The NH_2 group is planar in all cases. The NHD MECI geometries are in good agreement with the data calculated for simple alkyl amines. At the MRCI-(6/6) level, the NHD MECIs are lower in energy than the vertical excitation energies by 0.64 and 0.47 eV for conformer A and 0.92 and 0.58 eV for conformer B.

The hydrogen-transfer S_1/S_0 MECI (HT MECI) also represents one of the S_1 local minima. The structure of the HT MECI is depicted in Figure 2. Only conformer A has a suitable hydrogen-bonding arrangement in this respect, whereas conformer B would have to undergo a substantial conformational change to reach the crossing point. The energy of the HT MECI is at the MRCI(6/6) level 1.24 eV lower than the vertical excitation energy necessary to reach the S_2 state. It is also 0.19 eV higher than the nπ^*-state minimum. The route for conformer A from the nπ^*-state minimum to HT MECI is accompanied by a barrier. The transition point is at the MRCI-(6/6) level 0.43 eV higher than the nπ^*-state minimum. The HT MECI correlates to two ground-state products—the global minimum and a product with the transferred hydrogen •NH−CH_2−C(•)$(OH)_2$ biradical. The latter one is a metastable structure which is 3.85 eV higher in energy than the ground-state global minimum (at the MRCI(6/6) level).

4. Discussion

Possible Photochemical Pathways. The major features of the PES are schematically summarized in Figure 4.

On the basis of the previous results, possible photochemical processes can be proposed. Since the S_2 and S_1 states are close in energy in the FC region, the photochemical routes starting from both states are discussed.

After optical excitation to the S_2 state the wave packet approaches the S_2 minimum, which is also the S_2/S_1 MECI.

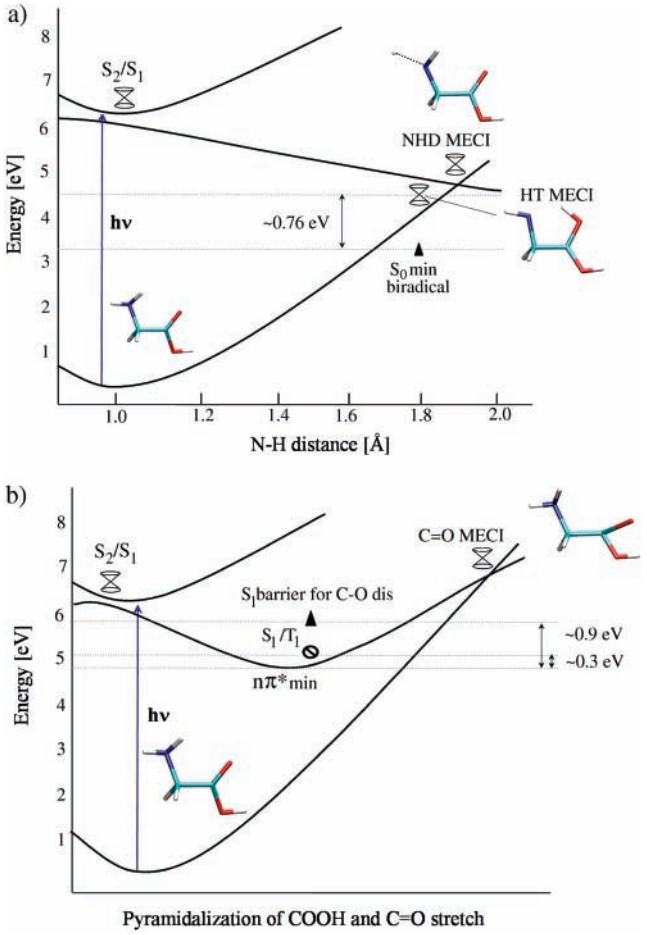

Figure 4. Illustration of possible photochemical processes: (a) possible pathways in the nσ^* state leading to the HT MECI or NHD MECI; (b) possible channels in the nπ^* state.

The initial wave packet is then funneled to the S_1 state. This process is supposed to happen on a femtosecond scale. The wave packet is consequently divided and evolves on the S_1 state having either $n_N \rightarrow \sigma^*$ or $n_O \rightarrow \pi_{CO}^*$ character (see Figure 4).

When excited to the S_1 state, the initial wave packet is put in the proximity of the S_2/S_1 MECI, which also represent the S_2 state minima for both conformers A and B. When passing through this region the initial wave packet can again be divided into a part evolving on the S_1 state having $n_O \rightarrow \pi_{CO}^*$ character and a part evolving on the state having $n_N \rightarrow \sigma^*$ character (see Figure 4). Part of the wave packet can be temporarily trapped on S_2 when passing through the S_2/S_1 region.

The processes in the nσ^* state will be discussed first. All graphs in Figure 5 are given for conformer A because the profiles for conformer B are fundamentally the same for N−H dissociation and C═O stretching (there is no hydrogen transfer in the case of the B conformer). Since the state is dissociative with respect to the N−H bond, N−H bond elongation results in either dissociation of the N−H bond or hydrogen transfer (see Figure 4). In the case of N−H bond dissociation the wave packet is funneled through the S_1/S_0 crossing point to the ground state. The mechanistic paths constructed by LICC between the FC point and the NHD MECI (lower in energy for conformer A) at the MRCI(6/6) level are depicted in Figure 5a. The FC region (with the N−H bond of a length of 1.001 Å) is in proximity of the S_2/S_1 crossing point. There is a barrier on the interpolation curve between the FC point and the NHD MECI. The position and height of the barrier is independent of whether we interpolated in internal coordinates or Cartesian space. When

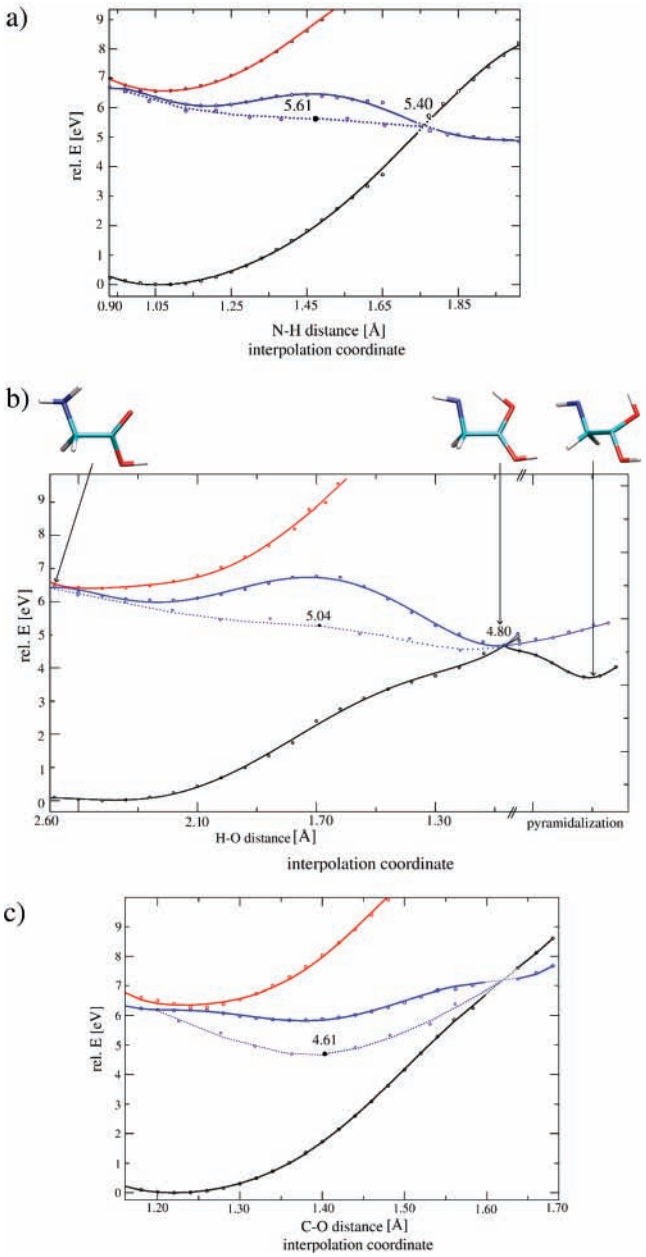

Figure 5. Interpolation between the FC point and the MECIs (solid lines): (a) N−H bond dissociation, (b) hydrogen transfer, and (c) C═O stretch and pyramidalization of the carboxyl group at the MRCI-(6/6) level. The *x* axis represents the interpolation coordinate (in the pictures, the interpolation coordinate is accompanied by the most relevant bond length). The black curve denotes the ground state S_0, the blue line is S_1, and the red curve is S_2. The dotted line is the interpolation between the FC point and the optimized structure corresponding to the top of the barrier. In the case of b the picture is divided into two parts, each having different interpolation coordinates. The first part shows the interpolation between the FC point and the conical intersection; the second part is between the conical intersection and the optimized S_0 geometry with the transferred hydrogen. All interpolations are for conformer A.

the LICC between the FC point and the optimized structure corresponding to the top of the barrier (with the N−H distance being 1.45 Å) is performed, the LICC curve becomes barrierless (see the dotted line in Figure 5a). The difference between the two curves (the blue solid line and the blue dotted line, Figure 5a) suggests that the processes are not straightforward and that some rearrangement of the structure is involved. The wave packet can thus be trapped in the entropical bottleneck, and many vibrations can occur in the nσ* state before the dissociation reaction is completed. The dissociation process is supposed to occur on a femtosecond timescale.

As mentioned before, N−H bond elongation can also result in hydrogen transfer to the carboxyl group. The reaction path obtained by the LICC between the FC point and the HT MECI (conformer A) is depicted in Figure 5b. Like in the case of N−H bond dissociation, the HT MECI is behind a barrier on the interpolation curve. The barrier also vanishes (the dotted line in Figure 5b) if the LICC is performed between the FC point and the optimized structure corresponding to the top of the barrier (with the H−O distance being 1.7 Å). It again suggests a barrierless route for this reaction. The products resulting from funneling of the wave packet through the HT MECI can be either the ground-state minimum or the •NH−CH_2−C(•)$(OH)_2$ biradical (see the second part of Figure 5b). Only the A-type structure has a suitable hydrogen-bonding arrangement for this process. Since the photodynamical process is supposed to be ultrafast, interconversion between the A and B type of structures would thus not be observed and the photodynamics would be conformationally dependent.

The processes in the nπ* state of glycine to a large extent parallelize the acetic acid behavior. Excitation into the π_{CO}* antibonding orbital causes pyramidalization of the carboxyl heavy atom backbone and elongation of the C═O bond, which is characteristic for the nπ*-state minima. The C═O stretch MECIs structures are different from the nπ*-state minima and energetically inaccessible (being more than 1 eV higher than the S_2 vertical excitation energies). The interpolation between the FC point and the C═O stretch MECI at the MRCI(6/6) level is given in Figure 5c. The reaction pathway between the FC point (for the C═O bond with a length of 1.209 Å) and the C═O stretch MECI is ascending. The same is true for the reaction path between the nπ*-state minimum and the C═O stretch MECI (the dotted line in Figure 5a). Decay via the HT MECI or the NHD MECIs is certainly possible, but both processes are accompanied by a rather high barrier (see Figure 3).

Like in the case of acetic acid, there are two more processes that can play a role in the nπ* state: ISC to the lowest triple state and direct C−O dissociation on the PES of the nπ* state. Even though the nπ*-state minima (for both conformers A and B) and the S_1/T_1 structures (for conformers A and B, see Figure 2) are close in conformational space and energy, the process is expected to be rather slow. A detailed investigation of the ISC processes and processes taking place in the lowest triplet state is not within the scope of the presented study. These processes occur well above the femtosecond time scale. Direct dissociation of the C−O bond on the nπ*-state PES is an over-the-barrier process (the height of the barrier is 0.94 eV). After quenching to the nπ*-state minimum basin the further processes possible are expected to be comparatively slow.

Reaction Pathways from ab Initio Dynamics. The static ab initio calculations discussed in the preceding sections have provided suggestions about possible photochemical routes. We identified ultrafast processes that can take place after excitation to the two lowest-lying states. To obtain a more detailed picture of the photochemical processes, we complemented the ab initio calculations with ab initio molecular-dynamics simulations.

In particular, we addressed the following questions: (i) how the initial wave packet splits between the nπ* and nσ* states, (ii) what the duration of the ultrafast processes is, (iii) whether there is any difference between the dynamics starting from the S_2 and S_1 states, and (iv) whether there is any population trapping in the S_2 state. (v) The most tempting question regards

TABLE 3: Branching Ratio of the Initial Wave Packet (%)[a]

	A		B	
	S_1	S_2	S_1	S_2
nπ* minimum	75	90	85	90
N−H dissociation	25	10	15	10
H transfer	0	0	0	0

[a] The branching ratio is given for the case when both the S_1 and S_2 states were initially populated. nπ* minimum refers to the trajectories that ended in the nπ* state minimum basin. N−H bond dissociation refers to the trajectories that followed the pathway to the NHD MECI and H transfer to the trajectories that followed the pathway to the HT MECI.

the importance of a hydrogen-transfer channel that would make the glycine photodynamics conformationally dependent. It is evident from the ab initio calculations that the hydrogen-transfer channel is energetically preferred.

The S_2 and S_1 states nearly intersect in the FC region. As a result, it is difficult to discern to which state the molecule is promoted after optical excitation. In our dynamical simulations we therefore populated both states equally (10 initial trajectories) for each conformer.

The results obtained after excitation to the S_2 state will be discussed first. The AIMS results for both conformers A and B show that S_2/S_1 degeneracy is achieved almost immediately. Evolution of the S_2/S_1 energy gap for conformer A is depicted in Figure 2S. The decay of the population on the S_2 is very rapid. On the basis of the AIMS simulations the S_2 state lifetime is less than 100 fs. The region of the crossing point is reached after the NH_2 group has been planarized. The small population in the S_2 state at the end of the simulation arises from the imposed restrictions that the basis can spawn only if the population exceeds a certain threshold. The population in the S_1 state is accumulated within 100 fs. The initial wave packet is divided into two parts. The majority (90% of the initial wave function for both the conformers A and B, see Table 3) has $n_O \rightarrow \pi_{CO}$* character. A major part of the wave packet is directed to the nπ*-state minimum. In the course of our simulation (500 fs) this part of the wave packet remains trapped in the nπ*-state minimum basin, and no further dynamical evolution of the wave packet has been observed. Note, however, that the nπ*-state minimum is somewhat overstabilized at the SA3-CAS-(6/7)SCF level (see Table 2). This disfavors possible decay channels.

The second part (10% for both the conformers A and B, see Table 3) is of $n_N \rightarrow \sigma$* character and evolves in the direction to the S_1/S_0 intersection region. It concerns typically 3−4 trajectories having significant population out of ∼70 total spawns. The trajectories reached the S_1/S_0 intersection region within 400 fs from the beginning of the simulation. At the end of the simulation the population of the S_0 state for both the conformers A and B was slightly below 10% of the initial wave function. All trajectories that were spawned on S_0 followed the N−H bond dissociation pathway.

Excitation to the S_1 state corresponds to promotion of the system to the state of $n_O \rightarrow \pi_{CO}$* character. The wave packet touches the S_2/S_1 MECI, and part of the wave packet is redirected to the nσ* state. When populating the S_1 state a slightly larger fraction of the initial wave packet (as compared to the S_2-state population) is of $n_N \rightarrow \sigma$* character (25% of the initial wave function for the A conformer and 15% of the initial wave function for the B conformer, see Table 3). This part of the population is completely funneled to the ground state via the NHD MECI; as a result the N−H bond dissociates. The trapping of some population in the S_2 state for a short period

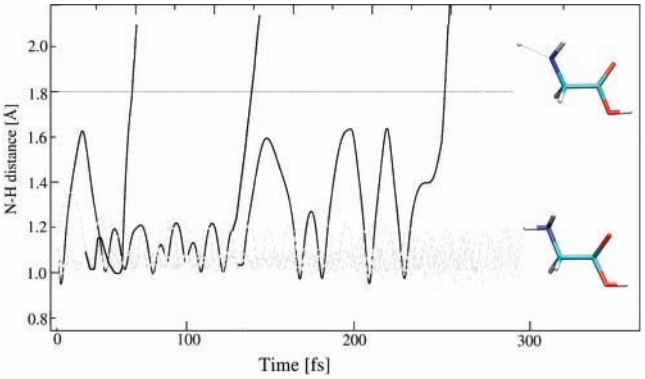

Figure 6. N−H bond distance as it evolves in time for 10 representative trajectories initially placed on S_1. The black solid lines represent the trajectories that followed the N−H dissociation pathway. The gray lines represent the trajectories that followed the path to the nπ*-state minimum. The dotted line is the N−H bond distance when the region of conical intersection is reached. The data are for conformer A.

of time has also been observed. In particular, 5% of the initial S_1 population was temporarily trapped on the S_2 surface for 10−20 fs. The time evolution of the N−H bond distance is depicted in Figure 6. NH_2-group vibrations of high amplitude are characteristic for all trajectories that reached the S_1/S_0 intersection region. It can be seen in Figure 6 that several vibrations occur before the S_1/S_0 intersection region is reached. No fundamental difference between the dynamics starting from the S_1 and S_2 states has thus been observed based on the dynamical results.

We have not recorded any passage through the HT MECI in our simulations. Neither have we observed the hydrogen-transfer reaction channel in our extensive test calculations with various electronic wave functions. Even though the hydrogen-transfer process cannot be definitely ruled out, it has concerned only a minor reaction channel. The reason is not based on the energetics of the reaction but rather on the entropic factor. Indeed, the phase space volume leading to N−H bond dissociation into free space is seemingly larger than for the hydrogen-transfer channel. The situation can be very different in a confined protein environment.

5. Conclusions

The goal of this study has been to explore the photochemical processes following optical excitation of the glycine molecule into its two low-lying excited states. We estimated the reaction paths connecting these important points. On the basis of the electronic structure calculations we identified the following possible dynamical pathways (see also Figure 5).

1. Quenching Into the nπ*-State Minimum and Subsequent Slow Dynamics. The carboxyl group pyramidalizes and the C═O bond is elongated. After the nπ*-state minimum is reached, the following processes are possible: (i) IC to the S_0 state via the C═O stretch MECI, (ii) ISC to the lowest triplet state, (iii) direct C−O(H) dissociation, and (iv) transformation into the nσ* state. All these are either activated processes with a barrier exceeding 1 eV or spin forbidden (ISC). Therefore, these processes do not occur on the ultrafast time scale.

2. N−H bond Dissociation. Acquiring $n_N \rightarrow \sigma$* character leads to elongation of the N−H bond. If the hydrogen atom dissociates into free space, the free hydrogen and the remaining fragment are produced. In the course of the dissociation the system quenches to the ground state via the NHD MECI.

3. Hydrogen Transfer. The departing hydrogen in the nσ* state can also be trapped by an oxygen atom of the carbonyl

group. This process requires suitable steric arrangement, which is best fulfilled for conformer A. In this case, the population is funneled to the S_0 state via HT MECI. The wave packet splits at this intersection into two ground-state products: the global minimum and a metastable biradical.

In summary, glycine photochemistry combines the photochemical behavior of alkyl amines and carboxylic acids.

In the FC region the states are close in energy. The S_1 state is dominantly of $n_O \rightarrow \pi^*_{CO}$ character and the S_2 state of $n_N \rightarrow \sigma^*$ character. Electronic excitation will presumably populate both of these states. To evaluate the importance of the proposed mechanisms we performed ab initio molecular-dynamics simulations using the full multiple spawning algorithm. These calculations yielded the following results. (1) The first and second mechanisms dominate glycine photochemistry. Quenching to the $n\pi^*$-state minimum appeared to be a dominant route for our selection of the electronic wave function (SA3-CAS-(6/7)SCF). Dissociation of the N−H bond was observed on the time scale of several hundred femtoseconds. No other dynamical process has been observed for the part of the wave packet trapped in the $n\pi^*$-state minimum basin within the time scale of the simulation. (2) No significant dependence on the initially populated state was observed. In other words, the Kasha−Vavilov rule[73,74] was not violated. (3) Mechanism 3 has not been observed. Therefore, no conformational dependence was recorded.

In summary, electronic structure methods at different levels of theory combined with dynamical calculations provide an accurate mechanistic picture of glycine photochemistry. Combining the CASSCF mapping of the PES with subsequent energy refinements at the MRCI level proved to be a fruitful approach. The example of glycine also shows that it is potentially important for a certain class of systems to consider entropic effects, e.g., by MD simulations.

It would be desirable to extend the present study in several directions. The next logical step should be to study the photochemical behavior of peptides with a more restricted conformational space. Dynamical calculations with a more accurate electronic wave function would also be desirable. To fully understand all the details it is also necessary to extend the MD simulations to much larger timescales, e.g., by utilizing methods tailored for description of rare but important events.[75]

Acknowledgment. This work was supported by grants from the Ministry of Education of the Czech Republic (Center for Biomolecules and Complex Molecular Systems, grant no. LC512) and the Grant Agency of the Czech Republic (grant no. 203/05/H001) and part of the research project no. Z40550506. P.S. thanks the postdoctoral grant of the Grant Agency of the Czech Republic (grant no. 203/07/P449). He also appreciates numerous discussions on the subject of ab initio quantum dynamics in the Martínez group at the University of Illinois.

Supporting Information Available: Geometries of A−D, time evolution of $\Delta S_2/S_1$ energy difference, vertical excitation energies of A−D. This material is available free of charge via the Internet at http://pubs.acs.org.

References and Notes

(1) Crespo-Hernandez, C. E.; Cohen, B.; Hare, P. M.; Kohler, B. *Chem. Rev.* **2004**, *104*, 1977.
(2) Broo, A. *J. Chem. Phys. A* **1998**, *102*, 526.
(3) Schultz, T.; Samoylova, E.; Radloff, W.; Hertel, I. V.; Sobolewski, A. L.; Domcke, W. *Science* **2004**, *306*, 1765.
(4) Kim, N. J.; Jeong, G.; Kim, Y. S.; Sung, J.; Kim, S. K.; Park, Y. D. *J. Chem. Phys.* **2000**, *113*, 10051.
(5) Canuel, C.; Elhanine, M.; Mons, M.; Piuzzi, F.; Tardivel, B.; Dimicoli, I. *Phys. Chem. Chem. Phys.* **2006**, *8*, 3978.
(6) Abo-Riziq, A.; Grace, L.; Nir, E.; Kabelac, M.; Hobza, P.; De Vries, M. S. *Proc. Natl. Acad. Sci.* **2005**, *102*, 20.
(7) Plutzer, C.; Nir, E.; De Vries, M. S.; Kleinermanns, K. *Phys. Chem. Chem. Phys.* **2001**, *3*, 5466.
(8) Blancafort, L. *J. Am. Chem. Soc.* **2006**, *128*, 210.
(9) Cohen, B.; Crespo-Hernandez, C. E.; Kohler, B. *Faraday Discuss.* **2004**, *127*, 137.
(10) Serrano-Andrés, L.; Merchan, M.; Borin, A. C. *Chem. Eur. J.* **2006**, *12*, 6559.
(11) Langer, H.; Doltsinis, N. L. *Phys. Chem. Chem. Phys.* **2004**, *6*, 2742.
(12) Sobolewski, A. L.; Domcke, W.; Hattig, C. *Proc. Natl. Acad. Sci.* **2005**, *102*, 17903.
(13) Sobolewski, A. L.; Domcke, W. *Chem. Phys. Chem.* **2006**, **7**, 561.
(14) Gardner, E. P.; McMesby, J. R. *J. Phys. Chem.* **1982**, *86*, 2646.
(15) Tanaka, N.; Oike, J.; Kajii, Y.; Shibuya, K.; Nakata, M. *Chem. Phys. Lett.* **1995**, *232*, 109.
(16) Michael, J. V.; Noyes, W. A. *J. Am. Chem. Soc.* **1963**, *85*, 1228.
(17) Dunn, K. M.; Morokuma, K. *J. Phys. Chem.* **1996**, *100*, 123.
(18) Kassab, E.; Gleghorn, J. T.; Evleth, E. M. *J. Am. Chem. Soc.* **1983**, *105*, 1746.
(19) Singleton, D. L.; Paraskevopoulos, G.; Irwin, R. S. *J. Phys. Chem.* **1990**, *94*, 695.
(20) Peterman, D. R.; Daniel, R. G.; Horwitz, R. J.; Guest, J. A. *Chem. Phys. Lett.* **1995**, *236*, 564.
(21) Hunnicutt, S. S.; Waits, L. D.; Guest, J. A. *J. Phys. Chem.* **1991**, *95*, 562.
(22) Zhong, Q.; Poth, L.; Castleman, A. W., Jr. *J. Chem. Phys.* **1999**, *110*, 192.
(23) Fang, W. H.; Liu, R. Z; Zheng, X.; Phillips, D. L. *J. Org. Chem.* **2002**, *67*, 8407.
(24) Nguyen, M. T.; Sengupta, D.; Raspoet, G.; Vanquickenborne, L. G. *J. Phys. Chem.* **1995**, *99*, 11883.
(25) Duan, X.; Page, M. *J. Am. Chem. Soc.* **1995**, *117*, 5114.
(26) Liu, Z. F.; Siu, C. K.; Tse, J. S. *Chem. Phys. Lett.* **1999**, *314*, 317.
(27) Bludský, O.; Chocholoušová, J.; Vacek, J.; Huisken, F.; Hobza, P. *J. Chem. Phys.* **2000**, *113*, 4629.
(28) Suenram, R. D.; Lovas, F. J. *J. Am. Chem. Soc.* **1980**, *102*, 7180.
(29) Godfrey, P. D.; Brown, R. D. *J. Am. Chem. Soc.* **1995**, *117*, 2019.
(30) Shemesh, D.; Gerber, R. B. *J. Chem. Phys.* **2005**, *122*, 241104.
(31) *Computational Methods in Photochemistry*; Kutateladze, A. G., Ed.; Molecular and Supramolecular Photochemistry; **2005**; Vol. 13.
(32) Bernardi, F.; Olivucci, M.; Robb, M. A. *Chem. Soc. Rev.* **1996**, *25*, 321.
(33) Garavelli, M.; Berbardi, F.; Olivucci, M.; Vreven, T.; Klein, S.; Celani, P.; Robb, M. A. *Faraday Discuss.* **1998**, *110*, 51.
(34) Garavelli, M. *Theor. Chem. Acc.* **2006**, *116*, 87.
(35) Robb, M. A.; Garavelli, M.; Olivucci, M.; Bernardi, F. *Rev. Comput. Chem.* **2000**, *15*, 87.
(36) Olsen, S.; Toniolo, A.; Ko, C.; Manohar, L.; Lamothe, K.; Martínez, T. J. *Computational Photochemistry*; Elsevier: New York, 2005.
(37) Punwong, C.; Owens, J.; Martínez, T. J. *Biophys. J.* **2005**, *88*, 530A.
(38) Röhrig, U. F.; Guidoni, L.; Röthlisberger, U. *Chem. Phys. Chem.* **2005**, *6*, 1836.
(39) Toniolo, A.; Olsen, S.; Manohar, L.; Martínez, T. J. *Faraday Discuss.* **2004**, *127*, 149.
(40) Migani, A.; Robb, M. A.; Olivucci, M. *J. Am. Chem. Soc.* **2003**, *125*, 2804.
(41) Groenhof, G.; Bouxin-Cademartory, M.; Hess, B.; De Visser, S. P.; Berendsen, H. J. C.; Olivucci, M.; Robb, M. A. *J. Phys. Chem. A* **2004**, *126*, 4228.
(42) Yarkony, D. R. *J. Phys. Chem.* **2001**, *105*, 6277.
(43) Yarkony, D. R. *Rev. Mod. Phys.* **1996**, *68*, 985.
(44) Robb, M. A.; Bernardi, F.; Olivucci, M. *Pure Appl. Chem.* **1995**, *67*, 783.
(45) *Computational Photochemistry*; Olivucci, M., Ed.; Theoretical and Computational Chemistry; Elsevier: New York, 2005; Vol. 16.
(46) Dreuw, A.; Head-Gordon, M. *Chem. Rev.* **2005**, *105*, 4009.
(47) Levine, B. G.; Ko, C.; Quenneville, J.; Martínez, T. J. *Mol. Phys.* **2006**, *104*, 1039.
(48) Andersson, K.; Malmquist, P. A.; Roos, B. O.; Sadlej, A. J.; Wolinski, K. *J. Phys. Chem.* **1990**, *94*, 5483.
(49) Andersson, K.; Malmquist, P. A.; Roos, B. O. *J. Phys. Chem.* **1992**, *96*, 1218.
(50) Tully, J. C.; Preston, R. K. *J. Chem. Phys.* **1971**, *55*, 562.
(51) Mitric, R.; Bonacic-Koutecky, V.; Pittner, J.; Lischka, H. *J. Chem. Phys.* **2006**, *125*, 024303.
(52) Zechmann, G.; Barbatti, M.; Lischka, H.; Pittner, J.; Bonacic-Koutecky, V. *Chem. Phys. Lett.* **2006**, *418*, 377.
(53) Hack, M. D.; Truhlar, D. J. *J. Phys. Chem.* **2000**, *104*, 7917.

(54) Volobuev, Y. L.; Hack, M. D.; Topaler, M. S.; Truhlar, D. J. *J. Chem. Phys.* **2000**, *112*, 9716.
(55) Doltsinis, N. L.; Marx, D. *Phys. Rev. Lett.* **2002**, *88*, 166402.
(56) Tapavicza, E.; Tavernelli, I.; Röthlisberger, U. *Phys. Rev. Lett.* **2007**, *98*, 023001.
(57) Hack, M. D.; Jasper, A. W.; Volobuev, Y. L.; Schwenke, D. W.; Truhlar, D. J. *J. Phys. Chem. A* **2000**, *104*, 217.
(58) Ben-Nun, M.; Martínez, T. J. *J. Chem. Phys.* **1998**, *108*, 7244.
(59) Ben-Nun, M.; Quenneville, J.; Martínez, T. J. *J. Phys. Chem. A* **2000**, *104*, 5161.
(60) Ben-Nun, M.; Martínez, T. J. *Adv. Chem. Phys.* **2002**, *121*, 439.
(61) Perun, S.; Sobolewski, A. L.; Domcke, W. *Mol. Phys.* **2006**, *104*, 1113.
(62) Werner, H.-J.; Knowles, P. J.; Lindh, R.; Manby, F. R.; Schütz, M.; Celani, P.; Korona, T.; Rauhut, G.; Amos, R. D.; Bernhardsson, A.; Berning, A.; Cooper, D. L.; Deegan, M. J. O.; Dobbyn, A. J.; Eckert, F.; Hampel, C. and Hetzer, G.; Lloyd, A. W.; McNicholas, S. J.; Meyer, W. and Mura, M. E.; Nicklass, A.; Palmieri, P.; Pitzer, R.; Schumann, U.; Stoll, H.; Stone, A. J.; Tarroni, R. and Thorsteinsson, T. *MOLPRO*, version 2006.1, a package of ab initio programs.
(63) Levine, B.; Martínez, T. J. *FMSMolPro*.
(64) Barone, V.; Adamo, A.; Lelj, F. *J. Chem. Phys.* **1995**, *102*, 364.
(65) Neta, P.; Simic, M.; Hayon, E. *J. Phys. Chem.* **1970**, *74*, 1214.
(66) Wetlaufer, D. B. Ultraviolet spectra of proteins and amino acids. In *Advances in Protein Chemistry*; Academic Press: New York, 1962; Vol. 17.
(67) Vinogradov, I. P.; Dodonova, N. Y. *Opt. Spectrosc.* **1970**, *30*, 14.
(68) Snyder, P. A.; Vipond, P. M.; Johnson, W. C., Jr. *Biopolymers* **1973**, *12*, 975.
(69) McMillin, C. R.; Rippon, W. B.; Walton, A. G. *Biopolymers* **1973**, *12*, 589.
(70) Inagaki, T. *Biopolymers* **1973**, *12*, 1353.
(71) Osted, A.; Kongsted, J.; Christiansen, O. *J. Chem. Phys. A* **2005**, *109*, 1430.
(72) Serrano-Andrés, L.; Fülscher, M. *J. Am. Chem. Soc.* **1996**, *118*, 12200.
(73) Kasha, M. *Faraday Discuss.* **1950**, *9*, 14.
(74) Vavilov, S. I. *Z. Phys.* **1927**, *42*, 311.
(75) Bolhuis, P. G.; Chandler, D.; Dellago, C.; Geissler, P. L. *Ann. Rev. Phys. Chem.* **2002**, *53*, 291.